A Ti6Al4V functionalized with a quorum quenching enzyme and biocompatible in a Caenorhabditis elegans model system

Discover Materials

https://doi.org/10.1007/s43939-026-00749-6

Article in Press

A Ti6Al4V functionalized with a quorum quenching enzyme and biocompatible in a *Caenorhabditis elegans* model system

Received: 6 March 2026

Accepted: 29 May 2026

Published online: 06 June 2026

Cite this article as: Rossanese A., Curcic J., Malesevic M. *et al.* A Ti6Al4V functionalized with a quorum quenching enzyme and biocompatible in a *Caenorhabditis elegans* model system. *Discov Mater* (2026). https://doi.org/10.1007/s43939-026-00749-6

Anna Rossanese, Jovana Curcic, Milka Malesevic, Sara Ferraris, Andrea Cochis, Mirko Prato & Silvia Spriano

A Ti6Al4V functionalized with a quorum quenching enzyme and biocompatible in a *Caenorhabditis elegans* model system

Anna Rossanese[1], Jovana Curcic[2], Milka Malesevic[2], Sara Ferraris[1], Andrea Cochis[3], Mirko Prato[4,] Silvia Spriano[1]

[1]Applied Science and Technology, Politecnico di Torino, Torino, Italy

[2]Institute of Molecular Genetics and Genetic Engineering, University of Belgrade, Vojvode Stepe 444a, Belgrade 11042, Serbia

[3]Department of Health Sciences, Center for Translational Research on Autoimmune and Allergic Diseases–CAAD, Università degli Studi del Piemonte Orientale UPO, Novara, Italy

[4]Materials Characterization Facility, Istituto Italiano di Tecnologia, Genova, Italy

Abstract

Implant-associated infections, particularly periprosthetic joint infections, together with the rise of antibiotic-resistant pathogens such as *Pseudomonas aeruginosa*, highlight the need for alternative anti-infective strategies. In this study, we developed a functionalized Ti6Al4V surface based on the immobilization of a quorum-quenching lactonase enzyme (ST1-YtnP) to disrupt bacterial communication and biofilm formation.

The surface modification involved chemical etching, calcium incorporation, and enzyme immobilization. Successful functionalization was confirmed by surface charge analysis and compositional characterization, indicating changes consistent with enzyme grafting, along with increased surface hydrophilicity.

Biocompatibility was evaluated in vivo using a *Caenorhabditis elegans* model, demonstrating that the functionalized surfaces are non-toxic. Importantly, the potential toxicity associated with glycerol present in the enzyme solution was eliminated upon enzyme immobilization.

Overall, these results demonstrate that ST1-YtnP-functionalized Ti6Al4V represents a promising strategy for the development of antivirulence biomaterial surfaces, offering an approach to reduce infection risk without contributing to antibiotic resistance.

Keywords: lactonase; functionalization; titanium alloy; quorum quenching; glycerol; *Caenorhabditis elegans*; *Pseudomonas aeruginosa*

1. Introduction

With increasing life expectancy, the elderly population is growing, leading to a rise in chronic musculoskeletal conditions like osteoporosis. [1] These are often managed conservatively, but in severe cases, surgical interventions such as joint replacements become necessary. These surgeries require biomaterial-based prostheses that must meet high standards for biocompatibility, mechanical strength, osseointegration, corrosion, fatigue, and biofilm resistance. [2]

Titanium and its alloys, particularly Ti6Al4V (Grade 5), are widely used due to their excellent biocompatibility, mechanical properties, and ability to support tissue integration. [3] This alloy is the most used in a variety of biomedical devices, including orthopaedic and dental implants. [4]

Infections following biomedical device implantation remain a major healthcare challenge, particularly periprosthetic joint infections (PJI) after procedures like arthroplasty. [5] Treating PJI typically requires extended courses of broad-spectrum antibiotics, which can contribute to the escalating problem of antibiotic resistance (ABR). [6] ABR remains a growing global threat, increasing healthcare costs, and contributing to significant morbidity

and mortality. In the U.S. alone, approximately 3 million ABR infections are reported annually, while Europe sees around 33,000 related deaths. [7] This issue is compounded by widespread antibiotic misuse in both human and animal contexts. [8,9] Five major mechanisms contribute to ABR [10]: biofilms, multidrug efflux pumps, β-lactamases, aminoglycoside-modifying enzymes, and quorum sensing (QS). Biofilms create protective microenvironments where bacteria exhibit diverse resistant phenotypes and slow growth rates that render them less susceptible to antibiotics. [11,12] Addressing these mechanisms is critical.

QS is a microbial communication system that enables bacteria to detect and respond to changes in population density through the accumulation of small, low-molecular-weight signalling molecules known as autoinducers (AIs). [13] This process regulates a variety of microbial traits, including ABR, bioluminescence, biofilm formation, virulence, and sporulation. [12]

The modulation of AIs and all processes that disrupt QS are collectively referred to as quorum quenching (QQ). [14] QQ is a naturally occurring mechanism, employed by both QS-producing organisms and competing bacterial strains. [15] The goal of QQ strategy is to interfere with intercellular communication, thereby promoting a planktonic rather than transition into a sessile (biofilm) lifestyle. [16] This can be accomplished through various strategies, including inhibiting signal molecule biosynthesis, inactivating or degrading signalling molecules, blocking signal transduction by targeting signal receptors, and competitive inhibition. [17] Despite significant progress in the development of QS inhibitors and QQ enzymes, their translation into stable and biocompatible surface coatings for biomedical implants remains limited. In particular, the immobilization of enzymatic QQ agents on clinically relevant titanium alloys and the assessment of their in vivo biocompatibility are still insufficiently explored. Furthermore, the potential impact of enzyme stabilization strategies (e.g., glycerol-containing formulations) on biological responses is often overlooked. [18]

Therefore, this study aims to address these gaps by developing an effective functionalization protocol of a titanium surface with ST1-YtnP as a QQ enzyme and by evaluating the in vivo biocompatibility of the resulting surface. In this work, ST1-YtnP lactonase was selected as a QQ agent, since its enzymatic properties and its quorum quenching activity were demonstrated in a previous work. [19] The eventual toxicity associated with purified enzyme solutions, arising from glycerol, was also investigated.

C. elegans was used as a powerful in vivo model for assessing biocompatibility while aligning with the 3R principles, as it reduces reliance on vertebrate testing, refines experimental design with high-throughput assays, and replaces more ethically sensitive organisms.

2. Materials and methods

2.1 Samples preparation

Ti6Al4V (ASTM B348, Gr 5, Titanium Consulting & Trading, composition: Fe 0.13, C 0.011, N 0.01, H 0.002, O 0.15, Al 6.11, V 4.12, Ti balance) samples were prepared by sectioning cylindrical bars (10 mm in diameter) into disks 2 mm in thickness with an automatic cutter (IsoMet High Speed Pro, Buehler). Subsequently, the samples were polished using SiC abrasive paper up to 4000-grit with a polishing machine (LaboPol-2, Struers), followed by a thorough cleaning process involving acetone and ultra-pure water in an ultrasonic bath (2400 ETH S3, Sonica) for 10 minutes. Finally, the samples were air-dried under a biological hood for several hours to prevent any potential contamination: these samples will be named Ti64-MP (mirror polished) from now on.

2.2 Surface treatment

Subsequently, Ti64-MP samples underwent a thermo-chemical treatment (as described in Patent no. EP2214732 and in [20,21]), which involves the removal of the native oxide layer through acid etching in hydrofluoric acid

and a controlled oxidation process using hydrogen peroxide. Hydrogen peroxide oxidation was used to generate a surface layer rich in hydroxyl groups, exhibiting a nanoporous structure and strong adhesion. The samples after the chemical treatment were labelled as Ti64 CT (chemically treated).

2.3 Enzymatic functionalization

The ST1-YtnP enzyme was extracted at the Institute of Molecular Genetics and Genetic Engineering (IMGGE) in Belgrade, Serbia and already characterized. [19] To ensure its stability and viability, it was preserved in a glycerol solution.

Ti64 CT samples underwent a UV-C radiation treatment (UV BOX E 2/40H, Light Progress) for 1 hour to activate hydroxyl groups on the surface, then they were submerged in 1 mL of $CaCl_2$ solution with a final concentration of 0.292 g/L and incubated for 24 hours at 37°C to impart the samples' surface a positive charge to facilitate the functionalization. [22] These samples will be named Ti64 CT-Ca.

Subsequently, the functionalization solutions were prepared by mixing the purified recombinant ST1-YtnP enzyme with TRIS/HCl pH 7.1 and with 50% glycerol, which helps preserving the activity of the enzyme, obtaining a concentration of 200 µg/mL. This value comes from the calculation of MIC, which was set at 400 µg/mL [19]; considering that the bacteria will be in direct contact with the enzyme when they colonize the functionalized chemically treated titanium surface, with an increment of the efficacy of the antibacterial effect in comparison with a liquid environment, this concentration was halved. Then, a drop of 100 µL of the functionalization solution was deposited on the sample, and it was left for 2 hours at room temperature in a humid environment, created by placing a wet piece of paper along the inner edge of the Petri dish containing the samples, under a biological hood. Afterwards, the samples were rinsed in 1 mL of Milli-Q water for few seconds to eliminate the excess of functionalization solution from the

surface. From now on, these samples will be named Ti64 CT-Ca-ST1. The whole procedure is reported in *Figure 1*.

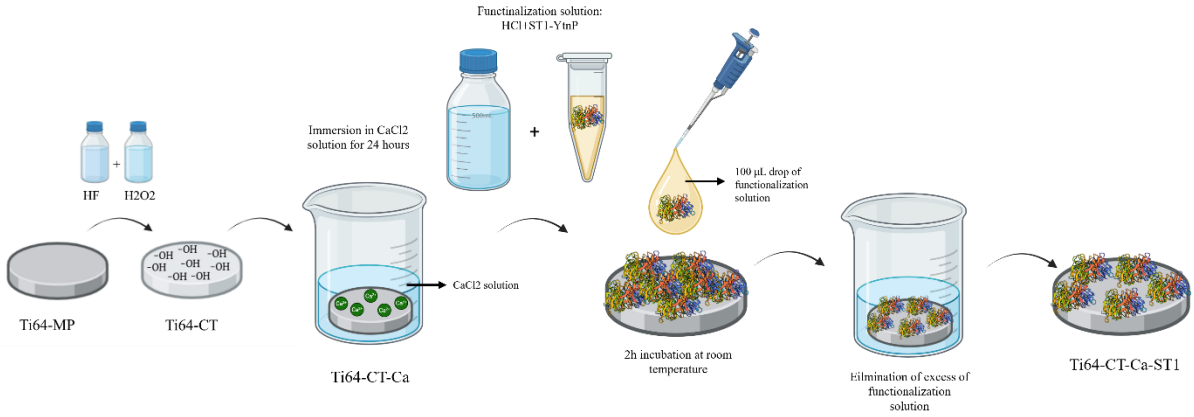

Figure 1: functionalization process of Ti6Al4V samples

2.4 Surface characterization

2.4.1 Contact Angle measurement

Surface wettability was evaluated using contact angle measurements performed with a DSA-100 (KRÜSS GmbH) instrument. The sessile drop method was employed to assess the wettability of Ti64 CT, Ti64 CT-Ca and Ti64 CT-Ca-ST1, specifically by measuring the angle formed between an ultra-pure water droplet (5 µL) and the sample surface. A photographic image of the droplet-surface interaction was captured to facilitate accurate contact angle determination. This measurement was performed in triplicate and a statistical analysis (one-way ANOVA) was performed.

2.4.2 Zeta (ζ) potential measurements

The zeta (ζ) potential of solid samples was determined using an electrokinetic analyser (SurPASS, Anton Paar GmbH, Austria) equipped with an adjustable gap cell. 0.001M KCl was used as electrolyte, and 0.05M HCl and 0.05M NaOH for basic and acid titrations, through the instrument automatic

titration unit. For each measurement, the titration in the acidic and in the basic range were carried out with two distinct couple of samples. Measurements were performed on Ti64 CT, Ti64 CT-Ca, and Ti64 CT-Ca-ST1 samples. The measurement is repeated four times for each pH point and mean and standard deviation are then calculated and plotted.

The zeta (ζ) potential of ST1-YtnP solution was measured using a dynamic light scattering system was used (Litesizer 500, Anton Paar, Gratz, Austria). As the electrolyte, KCl was added to the enzyme solution, to obtain a concentration of 1 mM. Titration curves were obtained by manually titrating the pH with 0.05 M NaOH or 0.05 M HCl. For each pH point the measurement is repeated three times.

2.4.3 X-ray Photoelectron Spectroscopy (XPS)

Two distinct samples (Ti64 CT and Ti64 CT-Ca-ST1) were analysed by XPS analysis (Axis Ultra^{DLD}, Kratos Analytical Ltd.) to examine differences in surface chemical composition. Both survey (0-1200 eV) and high-resolution spectra (on the main XPS peaks for C, O, N, Ti, Ca) were acquired, respectively at a pass energy of 160 eV (energy step of 1 eV) and of 20 eV (energy step of 0.1 eV). The binding energy scale calibration was performed by setting the position of the main C 1 s component at 284.8 eV (for C-C bonds).

2.5 Toxicity testing

2.5.1 Caenorhabditis elegans (C. elegans) strain, maintenance and synchronization

The *C. elegans* strain used in this study is AU37 (glp-4(bn2) I; sec-1(km4). Worms were cultured on standard nematode growth medium NGM agar plates (3 g/L NaCl, 2.5 g/L peptone, 17 g/L agar, supplemented with 1 mL each of 1 M $CaCl_2$, 1 M $MgSO_4$, and 5 mg/mL cholesterol, and 25 mL of 1 M potassium phosphate buffer (pH 6.0) seeded with *E. coli* OP50. NGM with

worms kept at 16°C. To obtain synchronized larvae, gravid hermaphrodites were treated with bleaching solution (1% NaOCl, 0.5 M NaOH), and isolated embryos were washed with M9 buffer (composed of 22 mM KH_2PO_4, 42 mM Na_2HPO_4, 86 mM NaCl, and 1 mM $MgSO_4$). and transferred to fresh NGM/OP50 plates. The plates were incubated at 16°C until the worms reached the L4 larval stage.

2.5.2 Toxicity of purified recombinant ST1-YtnP dissolved in 50% glycerol

L4 worms were gently washed from the plates using M9 buffer, collected in Falcon tubes, and allowed to settle. After removing the supernatant, worms were washed again with fresh M9 buffer. Toxicity testing was conducted in 96-well plates. Each well contained a final volume of 150 µL of S Basal Plus medium (100 mM NaCl, 50 mM potassium phosphate buffer, pH 6.0, and 5 µg/mL cholesterol) supplemented with purified recombinant ST1-YtnP lactonase dissolved in 20 mM Tris-HCl (pH 7.1) containing 50% glycerol in tested concentrations: 50, 100, 200, 400 µg/mL, and 1 mg/mL. Approximately 10–20 L4 worms were added per well. Incubation was conducted at 25°C to ensure temperature-sensitive sterility and with shaking at 150 rpm to maintain aeration. Negative controls contained 50% glycerol in Tris/HCl buffer without enzyme, along with the worms. The additional control contains just Tris-HCl buffer without glycerol (and without enzyme). Control contains just S Basal Plus medium. The number of live and dead worms was monitored at each 24 hours for three days and worms were considered dead if they showed no response to mechanical stimulation and had a rigid, elongated appearance. Each experiment was carried out in triplicate and repeated twice independently. The toxicity assay with *C. elegans* were conducted under blinded conditions. Specifically, the experimenter assessing the outcomes was not aware of the sample identity during data collection and analysis, thereby minimizing potential observer bias.

2.5.3 Toxicity of Ti64 CT-Ca-ST1

The toxicity assay was performed in sterile 24-well plates. Each well contained approximately 10–20 L4 worms suspended in 500 µL of S Basal Plus medium, consisting of S Basal Plus medium. Worms were exposed to Ti6Al4 CT-Ca-ST1 functionalized titanium disks, with one disk placed per well. As controls, two parallel conditions were included: (1) worms exposed to non-functionalized Ti64 CT-Ca disks, and (2) worms incubated in S Basal Plus medium only, without any titanium material. During the exposure phase, AU37 worms were incubated at 25°C to ensure sterility. Worm viability was monitored under a stereomicroscope at 24-hour time intervals during three days. Animals were classified as dead if they failed to respond to gentle mechanical stimulation and displayed a stiff, needle-like body posture. The toxicity assays with C. elegans were conducted under blinded conditions. Specifically, the experimenter assessing the outcomes was not aware of the sample identity during data collection and analysis, thereby minimizing potential observer bias. The toxicity assays with *C. elegans* were conducted under blinded conditions. Specifically, the experimenter assessing the outcomes was not aware of the sample identity during data collection and analysis, thereby minimizing potential observer bias. Each treatment and control condition were tested in triplicate and repeated twice independently.

3. Results and discussion

3.1 Surface characterization

3.1.1 Contact angle measurement

Surface wettability of samples at the different steps of the functionalization protocol (Ti64 CT, Ti64 CT-Ca, and Ti64 CT-Ca-ST1) was measured and summarized in *Table 1.*

Table 1: Contact angle measurements

Sample	***Contact Angle (°)***	

Ti64 CT	63.9 ± 0	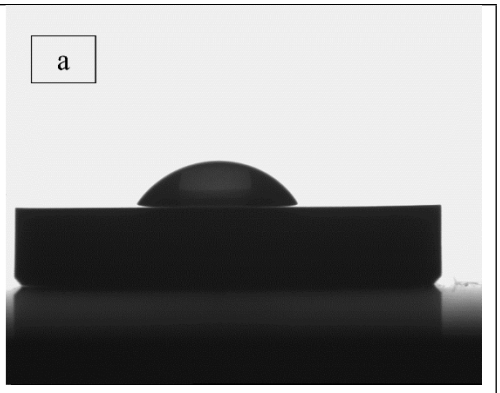
Ti64 CT-Ca	46.8 ± 17.1	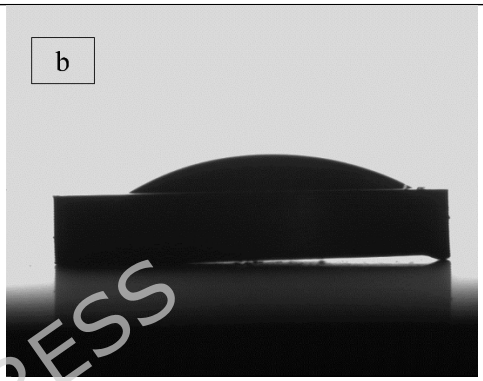
Ti64 CT-Ca-ST1	43.6 ± 8.5	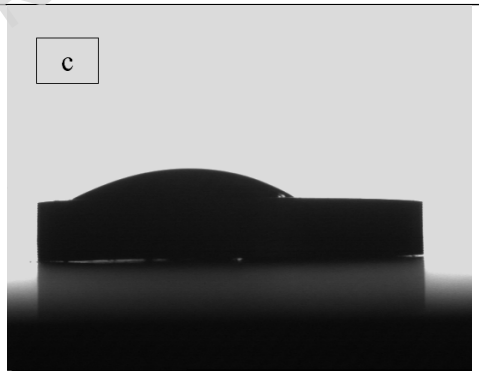

Contact angle measurement is a key method for evaluating surface modification efficacy, as it provides insights into surface wettability or hydrophilicity, properties that critically influence cell behavior, particularly cell adhesion. Surfaces with contact angles below 60° generally favor cell attachment, while high hydrophobicity increases the risk of bacterial adhesion.

The Ti64 CT sample (*Table 1a*) exhibited a contact angle of 63.9°, indicating moderate hydrophilicity, mainly due to the presence of hydroxyl groups on

the oxide layer due to chemical etching. Subsequent treatments, including UV exposure, calcium ion functionalization (Ti64 CT-Ca, *Table 1b*), and enzyme coating with ST1-YtnP (Ti64 CT-Ca-ST1, *Table 1c*), resulted in a progressive reduction in contact angle. UV treatment improves hydrophilicity by eliminating hydrophobic contaminants, while ST1-YtnP contributes to hydrophilicity due to its hydrophilic amino acid residues, such as glutamic acid, threonine, and lysine. Statistical analysis revealed a significant difference among the groups (one-way ANOVA, $p = 0.0033$). In conclusion, the obtained contact angle values indicate that cell adhesion is not prevented on the functionalized surface by any hydrophobicity. The small difference measured between Ti64 CT-Ca and the ST1-functionalized samples was not sufficient to confirm successful enzyme immobilization, which is why surface characterization was completed by the analyses presented below.

3.1.2 ζ potential measurement

ζ potential measurements were performed on the purified recombinant ST1-YtnP enzyme (in solution), Ti64 CT, Ti64 CT-Ca, and on the functionalized (Ti64 CT-Ca-ST1) samples, as described in section 2.4.1. The results, reported in *Figure 2*, show that ST1 exhibits a positive ζ potential at acidic pH values (around pH 3–5), likely due to the protonation of basic groups such as amines. As the pH increases, the ζ potential decreases sharply, reaching the isoelectric point near pH 6.05, and becomes negative at higher pH levels. This trend reflects the deprotonation of acidic groups, such as carboxyls, which can be exploited for the functionalization process. At the pH used for the functionalization (pH 7.1 - in TRIS/HCl buffer), the enzyme carries a net negative charge, facilitating its interaction with a positively charged surface. Conversely, positively charged $-NH_3^+$ groups of some amino acids (like Lys and Arg) are expected to be exposed and they can electrostatically interact with negatively charged functional groups.

Ti6Al4V CT has a high density of acidic -OH groups, which are completely deprotonated at any pH higher than pH 5.5, where the onset of the plateau

is observed. The IEP is below pH 2, evidencing a reactivity of the -OH groups as a strong acid. Functionalization with calcium ions (Ti64 CT-Ca) shifts the IEP to pH close to 3 by reducing the surface density of -OH groups, which interact with the positive Ca^{2+} ions. The functionalization with calcium ions is useful for further functionalization with ST1 at pH 7: positively charged -NH_3^+ groups of ST1-YtnP lactonase can interact with dissociated -OH groups of Ti64 CT-Ca, while the carboxylic deprotonated groups of the enzyme can interact with Ca^{2+} ions adsorbed on the surface.

The curve of Ti64 CT-Ca-ST1 shows that functionalization was effective and chemically stable. The observed changes in ζ potential values, the presence of a distinct IEP, and the altered curve profile confirm successful functionalization of the titanium surface with the ST1 enzyme. The IEP of Ti64 CT-Ca-ST1 shifts toward higher values than the two non-functionalized samples, as expected, because a smaller number of acidic -OH groups of the surface were exposed and ST1 has a higher IEP than Ti64 CT-Ca. Nonetheless, IEP is not the same as ST1-YtnP in solution, evidencing that the surface coverage by grafted ST1-YtnP molecules was not complete, so there still are some acid -OH groups influencing the IEP (lowering it).

Across most of the pH range, standard deviations in ζ potential remained low, indicating surface stability with no significant surface corrosion or release. Standard deviations are a bit larger in the acidic region, but this is not of interest for applications at the physiological pH. [23] Since standard deviation reflects surface reactivity, low values support the conclusion of a stable interface. Moreover, despite the high flow rates used during measurement, no abrupt changes in ζ potential were detected, implying that the enzyme remains firmly bound to the surface, likely through strong electrostatic interactions.

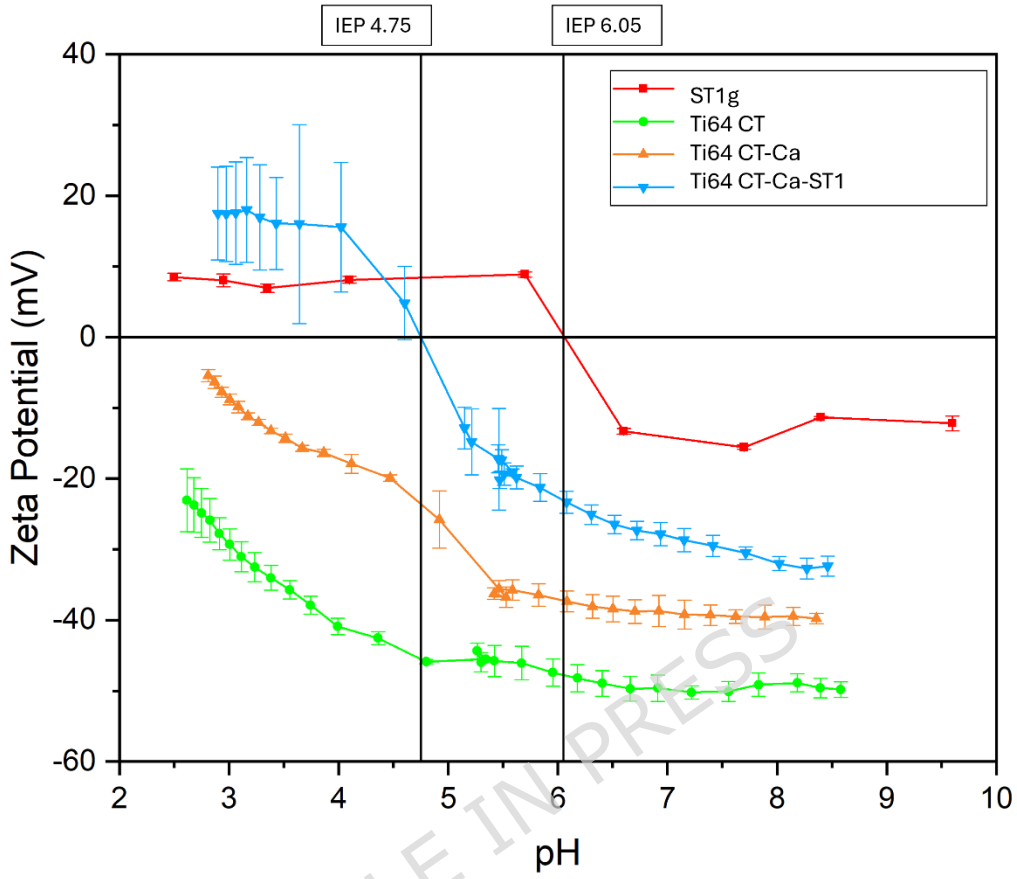

Figure 2: Zeta potential measurements of ST1g solution, Ti64 CT, Ti64 CT-Ca, Ti64 CT-Ca-ST1: the clear shift in the IEP between the non-functionalized and the functionalized samples and the different curve shape indicates that the enzyme is successfully grafted onto the titanium surface

3.1.3 X-ray Photoelectron Spectroscopy (XPS) measurements

XPS analysis was conducted on the Ti64 CT and on the Ti64 CT-Ca-ST1 samples to investigate their surface composition. In *Table 2,* the surface composition of each sample is summarized, and each detected element is reported in terms of atomic percentage. Moreover, an estimation of the atomic percentage of the ST1-YtnP lactonase is reported. [24]

The Ti64 CT sample (*Figure 3a - Table 2*), used as the reference, displayed characteristic signals of titanium and oxygen, along with minor nitrogen peaks likely due to unavoidable surface contamination. Oxygen was the

dominant surface element (55.8 at%), due to the formation of TiO_2 and surface hydroxyl groups (-OH) introduced during the chemical pre-treatment. A significant carbon signal (23.3 at%) was also present, which is commonly observed due to atmospheric exposure, as titanium readily adsorbs carbon-containing species from the environment. [25]

The Ti64 CT-Ca-ST1 sample (*Figure 3b – Table 2*) exhibited the same elemental signals as the reference sample, with the addition of calcium, with a surface concentration of 0.7 at%. Notably, a substantial increase in nitrogen content, from 2.6 at% in the reference to 13.1 at%, suggested the successful adsorption of ST1-YtnP lactonase. Additionally, the carbon content increased from 23.3 at% in Ti6A4 CT to 47.1 at%, in agreement with the carbon-rich composition of the ST1-YtnP enzyme. Concurrently, the relative amounts of oxygen and titanium decreased significantly, suggesting that the surface was effectively covered by the enzyme layer. While the oxygen signal on Ti64 CT-Ca-ST1 might have contributions from both the substrate and the ST1-YtnP enzyme, the attenuation of the Ti core-level signal can be used to estimate the thickness of the organic functionalization layer. This estimation is commonly based on an exponential attenuation model, assuming a uniform organic layer and using effective attenuation lengths appropriate for photoelectrons travelling through biomolecular matter. [26,27] Such XPS attenuation-based approaches have been widely applied to determine the thickness of protein and polymer films on solid substrates, [28–30] with the understanding that the resulting values represent effective thicknesses influenced by layer density and hydration.

The structure of ST1-YtnP lactonase, predicted by PSIPRED, indicates a transmembrane protein with an N-terminal extracellular domain and a C-terminal cytoplasmic domain, with most amino acid residues located extracellularly. [24] This results in a predominant atomic percentage of carbon (32%), followed by oxygen (10%) and nitrogen (9%).

In the present case, the area of the Ti 2p peaks reduced, after ST1-YtnP enzyme functionalization, to approximately 48% of that measured on the Ti64 CT sample (for reference, the area of the Ti $2p_{3/2}$ component went from ~ 27000 to ~13000 CPS·eV). Using an inelastic mean free path of 2.9 nm, calculated in [27] for amino acids and proteins, at the energy of Ti 2p peaks (kinetic energy of ~1000 eV), a thickness of approximately 2 nm was obtained. This estimation does not take into account hydration effects on the organic layer. The extracted coating thickness, combined with the detection of calcium as a bridging element between the surface and the enzyme, suggests that the functionalization process results in the formation of almost a monolayer of ST1-YtnP (the enzyme has an expected dimension of 3-5 nm). Unfortunately, no information about an eventual adsorption of glycerol can be derived from this analysis because it has no specific signal.

Table 2: Atomic percentage of the detected elements in Ti6A4 CT and Ti64 CT-Ca-ST1. Error bar = ±0.5

Sample	**Elements (at%)**				
	C	*O*	*N*	*Ti*	*Ca*
Ti64 CT	23.3	55.8	2.6	18.3	-
Ti64 CT-Ca ST1	47.1	31.4	13.1	7.7	0.7
ST1-YtnP (estimation)	32	10	9	-	-

In *Figure 3*, the high-resolution profiles are shown alongside the best results of the decomposition procedure. The obtained component positions and relative concentrations are summarized in *Table 3*. XPS peak profile fitting helps identify the chemical bonding environment of an element because its binding energy shifts with changes in chemical surroundings, revealing oxidation states and local bonding configurations. [31] In the profile-fitting analysis of the C region, both samples show that the C 1s signal can be decomposed into three peaks. In the case of the Ti64 CT sample, these are

attributed to aliphatic carbons (C-C, C-H), singly-bonded oxygen functionalities (C-O), and carboxyl groups (COOH). The first peak was dominant (75%), as expected for hydrocarbons from environmental contamination, while the relative concentration of C-O and COOH was lower (14% and 11%, respectively) [25,31] In the case of Ti64 CT-Ca ST1, the relative amount of carbon atoms associated with oxygen functionalities notably increased, reaching approximately 54% of the total carbon content. This was expected, considering that the enzyme is constituted of amino acids. It's also relevant to note that, on Ti64 CT-Ca ST1, the carbon component at higher binding energy, associated with carboxyl groups on Ti64 CT, shifted to lower binding energy, in agreement with reports on carboxylates and peptidic bonds. [31]

The Ti signal was attributed to TiO_2 in both samples, given the position of the main peak at (458.5±0.2) eV, indicating that the XPS penetration depth was insufficient to reach the underlying Ti metal beneath the oxide layer.

Looking at the oxygen region, the best fit was obtained with three components, namely a lattice-oxygen (O-Ti) component near ~530.0 eV, [32] a higher-binding-energy component at ~531.5 eV assigned to surface hydroxyls/adsorbed water, (acid -OH groups that cause the low IEP of the samples [21]), and an additional component at ~532–533 eV attributable to organic oxygen (carbonyl/carboxylate) or adventitious contamination. [31] Although the relative contents of the different components are quite similar on Ti64-CT and Ti64 CT-Ca ST1, the overall intensity of the oxygen signal for Ti64 CT-Ca ST1 is approximately half of what was observed on Ti64-CT.

The N region showed, in both samples, two peaks: a high-binding-energy peak assigned to protonated amine groups (NH_3^+) and a lower-binding-energy peak assigned to amine/amide groups. [31] They were almost equal in intensity on Ti64-CT (on which these species are most likely related to contaminations), while on Ti64 CT-Ca ST1, there was a prevalence of the amine/amide peak (about 93-95 % o the total nitrogen content).

The calcium signal is present only on sample Ti64 CT-Ca ST1, with the main peak at ~ 347.2 eV, which was attributed to Ca^{2+}, as expected. [33]

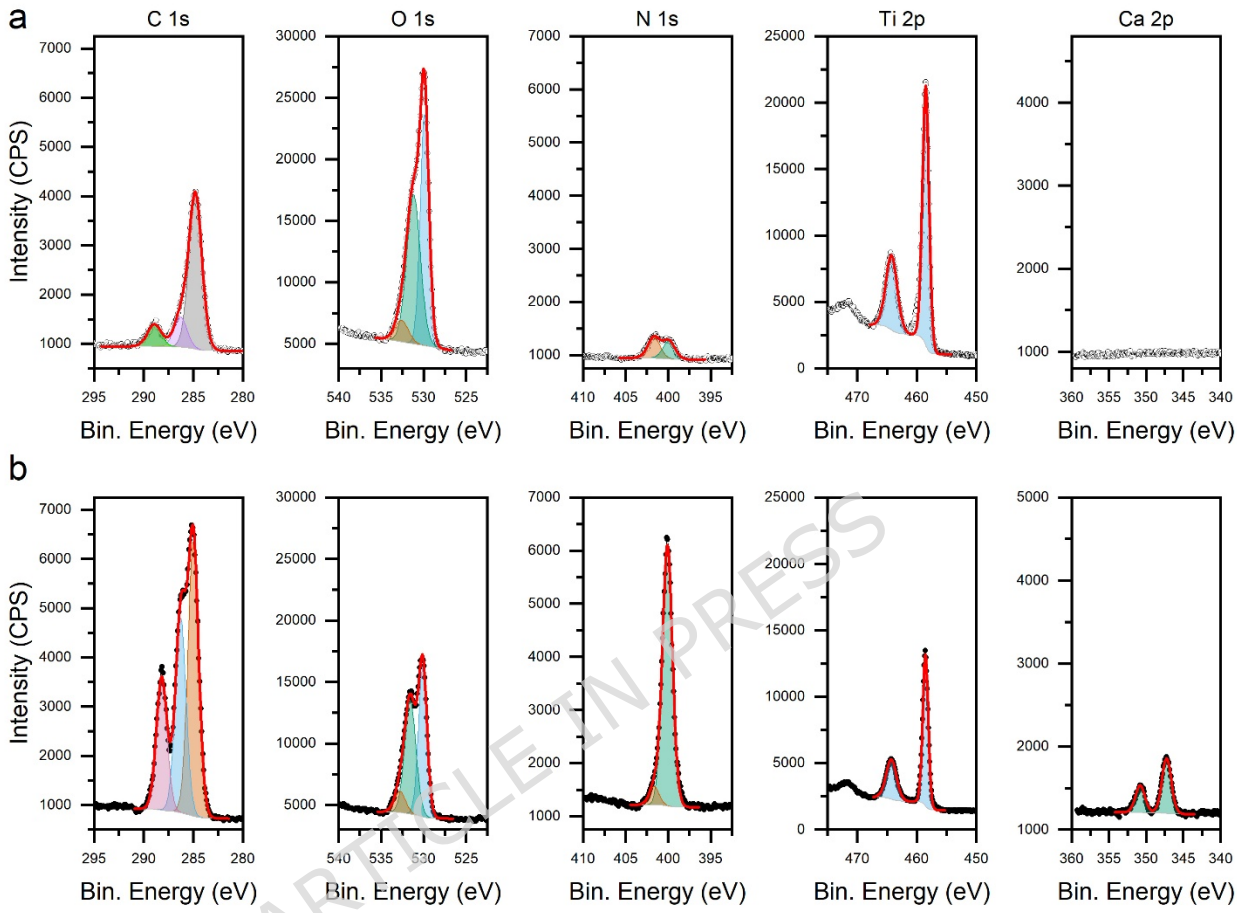

Figure 3: XPS measurement of a) Ti64 CT and b) Ti64 CT-Ca-ST1

Table 3 - XPS peak profile fitting of the C 1s, O 1s, N 1s, Ti 2p regions, showing binding energies (eV) and percentage areas for Ti64-CT and Ti64-CT-Ca-ST1

	Ti64-CT		***Ti64-CT-Ca-ST1***	
	Binding Energy (eV)	%Area	Binding Energy (eV)	%Area
C-C, C-H	284.8 ± 0.2	75	285.0 ± 0.2	46
C-O	286.4 ± 0.2	14	286.3 ± 0.2	32
O-C=O	288.9 ± 0.2	11	288.2 ± 0.2	22

	Ti64-CT	***Ti64-CT-Ca-ST1***

	Binding Energy (eV)	%Area	Binding Energy (eV)	%Area
O-Ti	529.9 ± 0.2	46	530.1 ± 0.2	46
-OH	531.2 ± 0.2	47	531.6 ± 0.2	45
C=O	532.6 ± 0.2	7	532.8 ± 0.2	9

	Ti64-CT		***Ti64-CT-Ca-ST1***	
	Binding Energy (eV)	%Area	Binding Energy (eV)	%Area
NH_3^+	401.7 ± 0.2	54	401.7 ± 0.2	7
NH_2*/(C=O)-NH-C*	399.9 ± 0.2	46	400.1 ± 0.2	93

	Ti64-CT		***Ti64-CT-Ca-ST1***	
	Binding Energy (eV)	%Area	Binding Energy (eV)	%Area
Ti(IV)-O	458.5 ± 0.2	100	458.5 ± 0.2	100

3.2 Toxicity analyses

3.2.1 In vivo toxicity of ST1-YtnP lactonase purified in glycerol-containing buffer

To evaluate the biosafety of the purified ST1-YtnP lactonase for potential in vivo applications, toxicity was tested using C. elegans AU37 temperature and stress-sensitive strain. The initial preparation of ST1-YtnP in 20 mM Tris-HCl buffer (pH 7.1) containing 50% glycerol resulted in acute toxicity at concentrations exceeding 100 µg/ml, on AU37 strains exhibiting rapid mortality within 24 hours of post-exposure (Figure 4). The results obtained at the highest tested concentration (1 mg/ml), presented in Supplementary Figure 6, further confirm the observed trend, showing rapid and complete mortality of C. elegans within 24 hours in glycerol-containing conditions, while control worms remained viable over the 72-hour period. Importantly,

similar toxic effects were observed in controls containing 50% glycerol, whereas no lethality was detected in worms exposed to an ST1-YtnP solution 20 mM in Tris-HCl buffer (pH 7.1 - control on the graph). These results indicate that glycerol, rather than the enzyme itself, was the primary cause of toxicity. Direct glycerol supplementation has been shown to reduce C. elegans longevity, likely through the modulation of glycerol transport and insulin/IGF-1 signaling pathways. [34] However, recent evidence suggests that the effects of glycerol are highly context-dependent, as the precise enzymatic regulation of internal glycerol levels can act as a critical metabolic buffer that influences health span under varying nutritional conditions. [35]

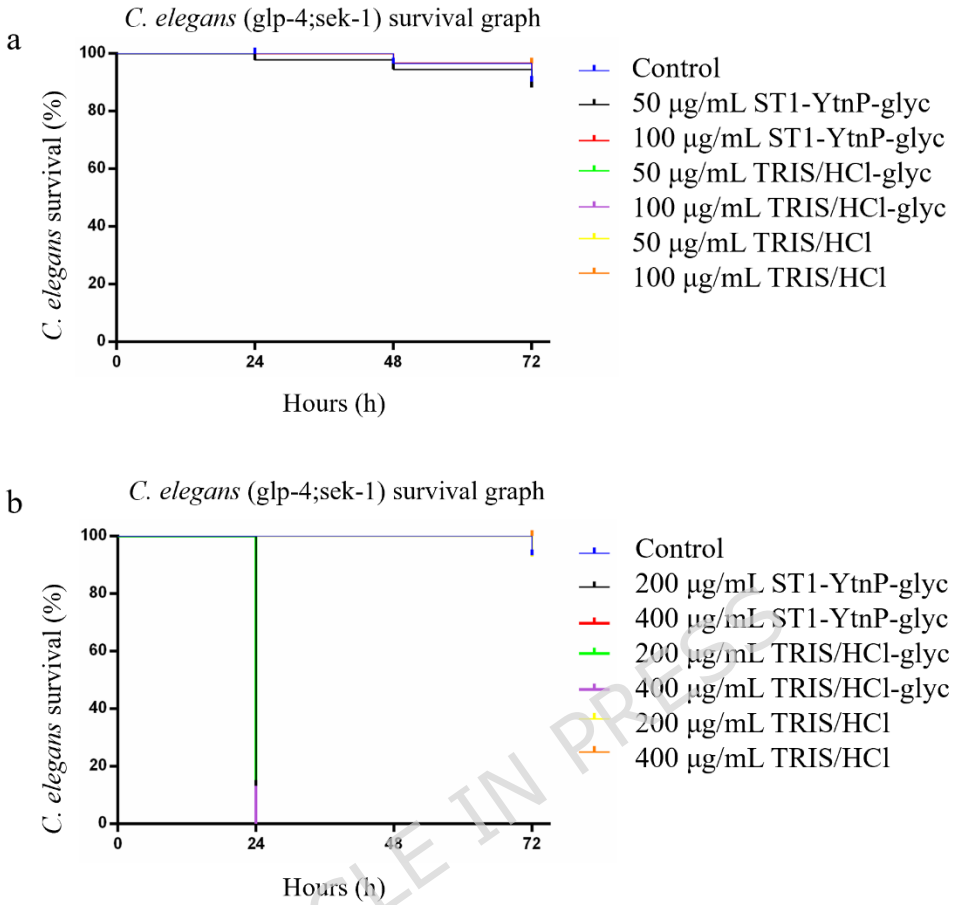

*Figure 4: Toxicity assessment of ST1-YtnP lactonase in C. elegans AU37 (glp-4; sek-1). Kaplan–Meier survival curves generated in GraphPad Prism Version 6.0 showing the effect of different concentrations (a) (50 and 100 µg/mL) and (b) (200 and 400 µg/mL) of ST1-YtnP lactonase with glycerol on nematode viability. Statistical analysis was performed using the log-rank (Mantel–Cox) test. No statistically significant differences in survival were observed between the untreated control and groups treated with 50 µg/ml ($p > 0.05$) and 100 µg/ml ($p > 0.05$) ST1-YtnP lactonase, indicating no observable toxicity at these concentrations. In contrast, treatment with higher concentrations 200 µg/mL and 400 µg/mL resulted in a significant reduction in survival (****$p < 0.0001$), with rapid mortality observed in both groups and control with glycerol. Data represent results from triplicate assays performed in two independent experiments.*

Although glycerol is widely used as a cryoprotectant and protein stabilizer due to its ability to prevent aggregation and preserve enzymatic activity, [36,37] its biological compatibility in whole-organism models such as *C. elegans* is limited. It was shown that even at concentrations as low as 1%, glycerol has been shown to reduce the lifespan of *C. elegans* by 23–36%, likely through disruption of osmoregulatory and metabolic processes, and induction

of proteotoxic stress. [38] Thus, while glycerol serves an important function in protein handling, its impact on biological models necessitates careful evaluation. Furthermore, a recent work [39] highlights that glycerol's stabilizing effects on enzymes are highly context-dependent. Factors such as enzyme class, concentration, pH, and immobilization strategy influence whether glycerol exerts a protective or destabilizing effect.

These findings highlight the importance of optimizing enzyme formulations for *in vivo* applications. Although glycerol is routinely used as an excipient in biochemical assays, its potential toxicity in whole-organism systems calls for empirically guided alternatives. Notably, extremophilic organisms such as *Bacillus licheniformis*, the native source of ST1-YtnP, naturally employ alternative cryoprotective mechanisms such as antifreeze proteins and compatible solutes, which may offer safer, biologically compatible options. [40] Future efforts should focus on developing glycerol-free formulations to improve the safety and applicability of enzyme-based biomaterials in clinical and environmental settings, avoiding any potential risks.

3.2.2 In vivo toxicity of ST1-YtnP-functionalized titanium discs in C. elegans

To evaluate the *in vivo* toxicity of ST1-YtnP lactonase-functionalized titanium discs (Ti64 CT-Ca-ST1), toxicity assays were performed using *C. elegans* AU37 strain. No statistically significant mortality was observed at AU37 worms exposed to the functionalized discs over 72 hours, compared to control conditions (*Figure 5*). Worms retained unchanged morphology and responsiveness to mechanical stimulation, indicating an absence of acute toxicity. So, the effective immobilization of ST1-YtnP lactonase on the surface of titanium discs did not interfere with *C. elegans* viability.

Previous studies on surface-functionalized titanium substrates with nanoparticles have demonstrated that surface functionalization can improve biological performance, [29] without inducing adverse biological responses,

even if the compound itself has potential toxicity, because of concentration effects and stabilization due to surface grafting. For instance, graphene-oxide-functionalized titanium discs exhibited good biocompatibility alongside antibiofilm activity without eliciting toxic effects. [30] In line with these findings, the absence of toxic effects observed in *C. elegans* exposed to ST1-YtnP-functionalized titanium discs further supports its biocompatible nature of this surface functionalization strategy, even if in the presence of glycerol in the solution. [41] This result suggests that probably only a limited amount of glycerol remained on the surface upon grafting and it was not directly released into the culture medium, reducing toxicity concerns even if the solution used for functionalization contained glycerol for the preservation of enzyme integrity.

Moreover, no nanoparticle was used in this work, thereby eliminating confounding effects related to particle internalization or systemic distribution. While metal-oxide nanoparticles like TiO_2 have raised concerns due to their potential to accumulate in reproductive tissues and cross biological barriers, thereby inducing oxidative stress and impairing fertility, [40] the inert behaviour of ST1-YtnP-functionalized discs highlights the importance of surface-engineered alternatives in minimizing toxicity risks. These findings highlight their promise as safe, surface-engineered biomaterials suitable for further exploration in preclinical models relevant to implantable medical devices.

Comparing these results with the literature, previous studies have explored various enzyme immobilization strategies to confer antibiofilm properties to biomaterial surfaces. For instance, medical-grade PU has been functionalized with acylase to reduce *P. aeruginosa* biofilm formation by approximately 60% under static conditions, while silicone substrates have been modified through layer-by-layer assembly with enzymes such as acylase or amylase to simultaneously disrupt QS signals and extracellular polysaccharides, enhancing inhibition of both mono- and multispecies biofilms. [42] Similarly,

covalent immobilization approaches using glycidyl methacrylate on PVC catheters have enabled stable binding of enzymes like lysozyme and acylase, effectively reducing S. aureus adhesion and degrading AHL-mediated QS signals, as demonstrated in C. violaceum. [43]

Overall, these findings demonstrate that ST1-YtnP-functionalized titanium surfaces constitute a promising proof-of-concept for enzymatic surface functionalization with potential antivirulence applications. However, further studies, including direct assessment of antibacterial activity and biofilm inhibition, are necessary to validate their performance as anti-virulence coatings in biomedical settings fully.

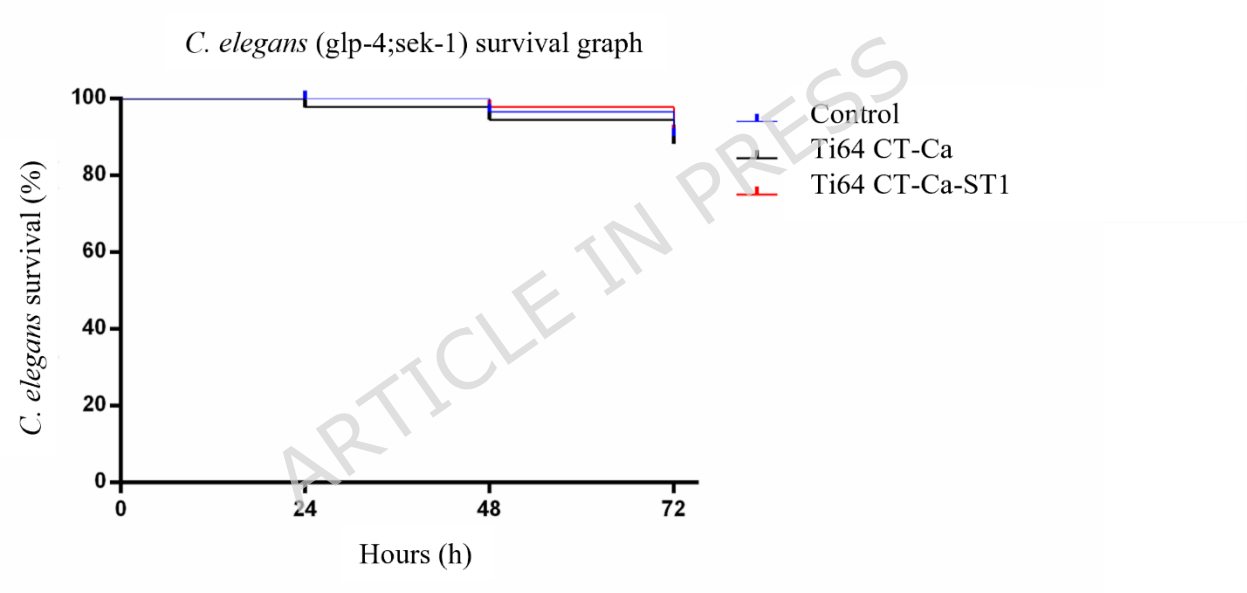

Figure 5: Toxicity assessment of functionalized Ti6Al4V discs in C. elegans (glp-4; sek-1). Kaplan–Meier survival curves generated in GraphPad Prism Version 6.0 showing the effect of Ti64 CT-Ca and Ti64 CT-Ca-ST1 samples on nematode viability over 72 hours. Statistical analysis was performed using the log-rank (mantel-Cox) test. No statistically significant differences in survival were observed between the untreated control group and groups treated with either Ti64 CT-Ca or Ti64 CT-Ca-ST1, indicating no observable toxicity of the tested materials under the experimental conditions. Data represent results from triplicate assays performed in two independent experiments.

4. Conclusions

The present work introduced an alternative strategy based on the immobilization of ST1-YtnP lactonase onto Ti6Al4V titanium surfaces via calcium-mediated electrostatic interactions, as confirmed by detailed surface

characterization. The functionalized surfaces demonstrated enhanced wettability. ST1 presence on the surface was confirmed by zeta potential and XPS analyses. Studies on the C elegans models evidence the non-toxicity of functionalized surfaces, even if glycerol-stabilized ST1 solutions were used for the grafting. This result indicates surface functionalization as an effective strategy for the local application of the enzyme, reducing potential glycerol-mediated toxicity. Although toxicity was observed in purified enzyme solutions due to glycerol, this effect was effectively mitigated through surface immobilization.

Supplementary material

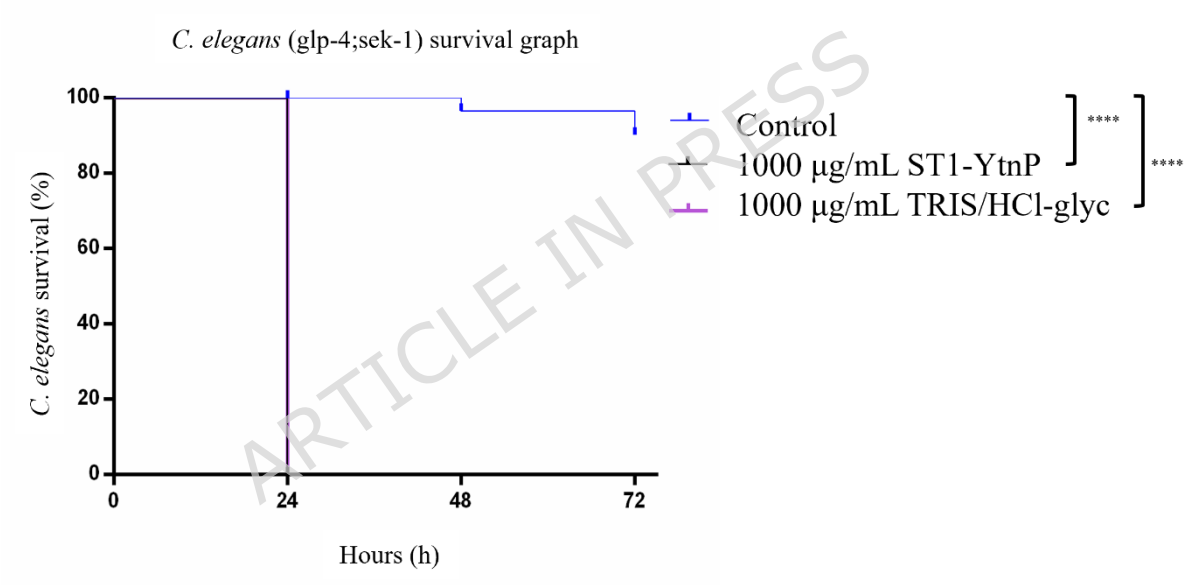

Figure 6: Toxicity assessment of ST1-YtnP lactonase in C. elegans AU37 (glp-4; sek-1)

Funding declaration

This research received no external funding and was conducted through collaborative efforts between the participating institutions.

Clinical trial number

Clinical trial number: not applicable.

Email addresses corresponding author

Anna Rossanese: anna.rossanese@polito.it

Silvia Spriano: silvia.spriano@polito.it

Milka Malesevic:_mmalesevic10@gmail.com

Declaration:

Ethical approval: not applicable

Consent to Participate: not applicable

Consent to Publish: not applicable.

Data Availability Statement

All data generated or analyzed during this study are included in this published article [and its supplementary information files].

References

[1] Quinn, J. *et al.* (2020). iScience Titanium for Orthopedic Applications: An Overview of Surface Modification to Improve Biocompatibility and Prevent Bacterial Biofilm Formation. https://doi.org/10.1016/j.isci.

[2] Biomedical Applications, A. *et al.* (2023). Biomedical Applications of Titanium Alloys: A Comprehensive Review. *Materials 2024, Vol. 17, Page 114*. https://doi.org/10.3390/MA17010114.

[3] Ferraris, S. and Spriano, S. (2016). Antibacterial titanium surfaces for medical implants. *Materials Science and Engineering: C*. https://doi.org/10.1016/J.MSEC.2015.12.062.

[4] Sarraf, M. *et al.* (2021). A state-of-the-art review of the fabrication and characteristics of titanium and its alloys for biomedical applications. *Bio-Design and Manufacturing 2021 5:2*. https://doi.org/10.1007/S42242-021-00170-3.

[5] Sloan, M. *et al.* (2018). Projected volume of primary total joint arthroplasty in the u.s., 2014 to 2030. *Journal of Bone and Joint Surgery - American Volume*. https://doi.org/10.2106/JBJS.17.01617,.

[6] Klasan, A. *et al.* (2021). Development of antibiotic resistance in periprosthetic joint infection after total knee arthroplasty. *Bone and Joint Journal*. https://doi.org/10.1302/0301-620X.103B6.BJJ-2020-1923.R1/LETTERTOEDITOR.

[7] Desai, A.N. *et al.* (2022). Antimicrobial Resistance and Human Mobility. *Infection and Drug Resistance*. https://doi.org/10.2147/IDR.S305078,.

[8] Hantouly, A.T. *et al.* (2024). High mortality rate and restricted mobility in above knee amputation following periprosthetic joint infection after total knee arthroplasty: A systematic review. *Archives of Orthopaedic and Trauma Surgery*. https://doi.org/10.1007/S00402-024-05578-X/TABLES/4.

[9] Reinhard, J. *et al.* (2024). In-hospital mortality of patients with periprosthetic joint infection: demographic, comorbidity, and complication profiles of 52,286 patients. *Bone & Joint Open*. https://doi.org/10.1302/2633-1462.54.BJO-2023-0162.R1.

[10] Lin, J. *et al.* (2015). Mechanisms of antibiotic resistance. *Frontiers in Microbiology*. https://doi.org/10.3389/fmicb.2015.00034.

[11] Michaelis, C. and Grohmann, E. (2023). Horizontal Gene Transfer of Antibiotic Resistance Genes in Biofilms. *Antibiotics 2023, Vol. 12, Page 328*. https://doi.org/10.3390/ANTIBIOTICS12020328.

[12] Abisado, R.G. *et al.* (2018). Bacterial Quorum Sensing and Microbial Community Interactions. *mBio*. https://doi.org/10.1128/MBIO.02331-17.

[13] Malešević, M. *et al.* (2019). Pseudomonas aeruginosa quorum sensing inhibition by clinical isolate Delftia tsuruhatensis 11304: involvement of N-octadecanoylhomoserine lactones. *Scientific Reports*. https://doi.org/10.1038/S41598-019-52955-3,.

[14] Rather, M.A. *et al.* (2022). Quorum Quenching: A Drug Discovery Approach Against Pseudomonas aeruginosa. *Microbiological Research*. https://doi.org/10.1016/J.MICRES.2022.127173.

[15] Wright, P.P. and Ramachandra, S.S. (2022). Quorum Sensing and Quorum Quenching with a Focus on Cariogenic and Periodontopathic Oral Biofilms. *Microorganisms*. https://doi.org/10.3390/microorganisms10091783.

[16] Mulat, M. *et al.* (2025). Multiple Strategies for the Application of Medicinal Plant-Derived Bioactive Compounds in Controlling Microbial Biofilm and Virulence Properties. *Antibiotics*. https://doi.org/10.3390/ANTIBIOTICS14060555.

[17] Yang, L. *et al.* (2021). A Meta-Analysis Reveals Opposite Effects of Biotic and Abiotic Stresses on Transcript Levels of Arabidopsis Intracellular Immune Receptor Genes. *Frontiers in plant science*. https://doi.org/10.3389/FPLS.2021.625729.

[18] Cimolato, C. *et al.* (2025). Quorum Sensing Model Structures Inspire the Design of Quorum Quenching Strategies. *IEEE Transactions on Molecular, Biological, and Multi-Scale Communications*. https://doi.org/10.1109/TMBMC.2025.3554671.

[19] Naga, N.G. *et al.* (2024). An insight on the powerful of bacterial quorum sensing inhibition. *European Journal of Clinical Microbiology and Infectious Diseases*. https://doi.org/10.1007/S10096-024-04920-W/METRICS.

[20] Curcic, J. *et al.* (2025). ST1-YtnP lactonase from extreme environment: A promising antivirulence agent against multidrug-resistant Pseudomonas aeruginosa. *Biomedicine & Pharmacotherapy*. https://doi.org/10.1016/J.BIOPHA.2025.118443.

[21] Ferraris, S. *et al.* (2016). Multifunctional commercially pure titanium for the improvement of bone integration: Multiscale topography, wettability, corrosion resistance and biological functionalization. *Materials Science and Engineering: C*. https://doi.org/10.1016/J.MSEC.2015.11.049.

[22] Ferraris, S. *et al.* (2011). Surface modification of Ti-6Al-4V alloy for biomineralization and specific biological response: Part I, inorganic modification. *Journal of Materials Science: Materials in Medicine*. https://doi.org/10.1007/S10856-011-4246-2/FIGURES/11.

[23] Reggio, C. *et al.* (2023). Functionalization of Ti6Al4V Alloy with Polyphenols: The Role of the Titanium Surface Features and the Addition of Calcium Ions on the Adsorption Mechanism. *Metals 2023, Vol. 13, Page 1347*. https://doi.org/10.3390/met13081347.

[24] Curcic, J. *et al.* (2025). ST1-YtnP lactonase from extreme environment: A promising antivirulence agent against multidrug-resistant Pseudomonas aeruginosa. *Biomedicine & Pharmacotherapy*. https://doi.org/10.1016/J.BIOPHA.2025.118443.

[25] Ferraris, S. *et al.* (2020). The mechanical and chemical stability of the interfaces in bioactive materials: The substrate-bioactive surface layer and hydroxyapatite-bioactive surface layer interfaces. *Materials*

Science and Engineering C. https://doi.org/10.1016/j.msec.2020.111238.

[26] Grey, L.H. *et al.* (2024). Defining the nature of adventitious carbon and improving its merit as a charge correction reference for XPS. *Applied Surface Science*. https://doi.org/10.1016/J.APSUSC.2024.159319.

[27] Tanuma, S. *et al.* (1994). Calculations of electron inelastic mean free paths. V. Data for 14 organic compounds over the 50–2000 eV range. *Surface and Interface Analysis*. https://doi.org/10.1002/SIA.740210302;ISSUE:ISSUE:DOI.

[28] Tan, Z. and Liu, Y. (2025). Electron inelastic mean free paths in a group of bioorganic compounds and liquid water over the energy range of 20–20,000 eV. *Nuclear Instruments and Methods in Physics Research Section B: Beam Interactions with Materials and Atoms*. https://doi.org/10.1016/j.nimb.2025.165781.

[29] Paynter, R.W. *et al.* (1984). XPS studies on the organization of adsorbed protein films on fluoropolymers. *Journal of Colloid and Interface Science*. https://doi.org/10.1016/0021-9797(84)90023-7.

[30] Aeimbhu, A. *et al.* (2005). Accounting for the size of molecules in determination of adsorption isotherms by XPS; exemplified by adsorption of chicken egg albumin on titanium. *Surface and Interface Analysis*. https://doi.org/10.1002/SIA.2120;PAGE:STRING:ARTICLE/CHAPTER.

[31] Cant, D.J.H. *et al.* (2021). Measurement of Peptide Coating Thickness and Chemical Composition Using XPS. *Methods in Molecular Biology*. https://doi.org/10.1007/978-1-0716-0928-6_14.

[32] Bagus, P.S. *et al.* (2023). Chemical significance of x-ray photoelectron spectroscopy binding energy shifts: A Perspective. *Journal of Vacuum Science and Technology A*. https://doi.org/10.1116/6.0003081.

[33] Bagus, P.S. *et al.* (2023). Chemical significance of x-ray photoelectron spectroscopy binding energy shifts: A Perspective. *Journal of Vacuum Science & Technology A*. https://doi.org/10.1116/6.0003081/2915551.

[34] De Guzman, A.C. V. *et al.* (2022). High-Glucose Diet Attenuates the Dopaminergic Neuronal Function in C. elegans, Leading to the Acceleration of the Aging Process. *ACS Omega*.

https://doi.org/10.1021/ACSOMEGA.2C03384/SUPPL_FILE/AO2C03384_SI_006.MPG.

[35] Possik, E. *et al.* (2023). Glycerol 3-phosphate phosphatase/PGPH-2 counters metabolic stress and promotes healthy aging via a glycogen sensing-AMPK-HLH-30-autophagy axis in C. elegans. *Nature Communications*. https://doi.org/10.1038/S41467-023-40857-Y;TECHMETA.

[36] Vagenende, V. *et al.* (2009). Mechanisms of Protein Stabilization and Prevention of Protein Aggregation by Glycerol. *Biochemistry*. https://doi.org/10.1021/BI900649T.

[37] Baeyens, B. and Bradbury, M.H. (1997). A mechanistic description of Ni and Zn sorption on Na-montmorillonite Part I: Titration and sorption measurements. *Journal of Contaminant Hydrology*. https://doi.org/10.1016/S0169-7722(97)00008-9.

[38] Hipkiss, A.R. (2010). Aging, proteotoxicity, mitochondria, glycation, NAD+ and carnosine: Possible inter-relationships and resolution of the oxygen paradox. *Frontiers in Aging Neuroscience*. https://doi.org/10.3389/FNAGI.2010.00010/XML.

[39] Braham, S.A. *et al.* (2021). Effect of Concentrated Salts Solutions on the Stability of Immobilized Enzymes: Influence of Inactivation Conditions and Immobilization Protocol. *Molecules 2021, Vol. 26, Page 968*. https://doi.org/10.3390/MOLECULES26040968.

[40] Marzban, N. *et al.* (2025). Smart integrated biorefineries in bioeconomy: A concept toward zero-waste, emission reduction, and self-sufficient energy production. *Biofuel Research Journal*. https://doi.org/10.18331/BRJ2025.12.1.4.

[41] Minghui, F. *et al.* (2023). Toxic effects of titanium dioxide nanoparticles on reproduction in mammals. *Frontiers in Bioengineering and Biotechnology*. https://doi.org/10.3389/FBIOE.2023.1183592/BIBTEX.

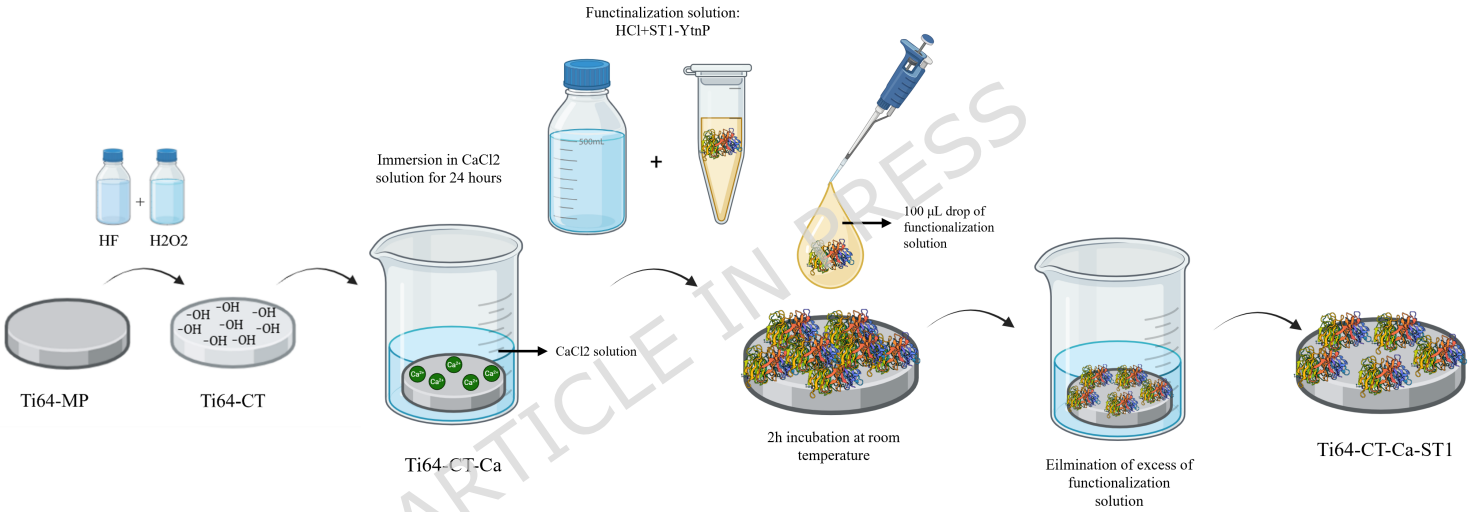

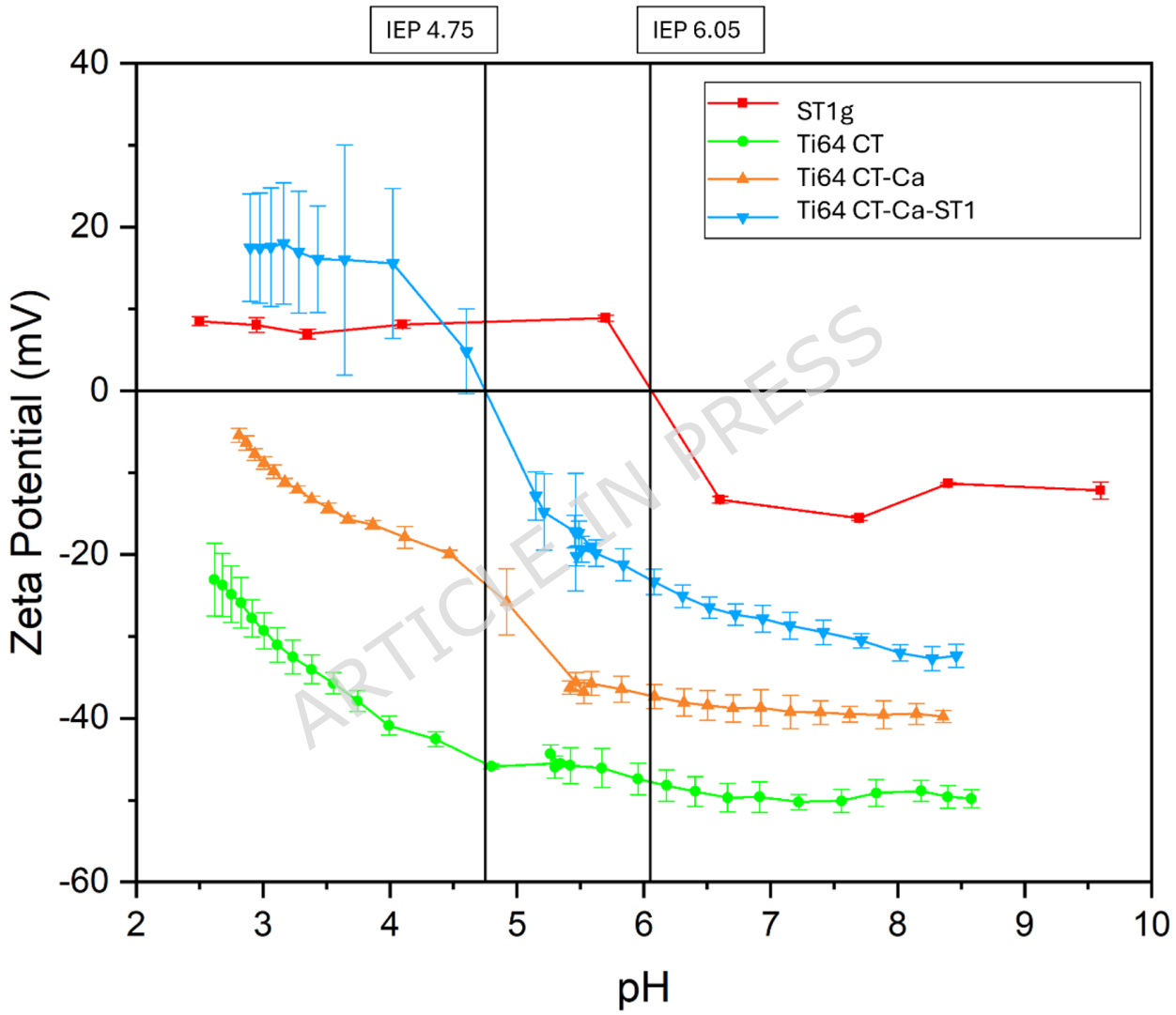

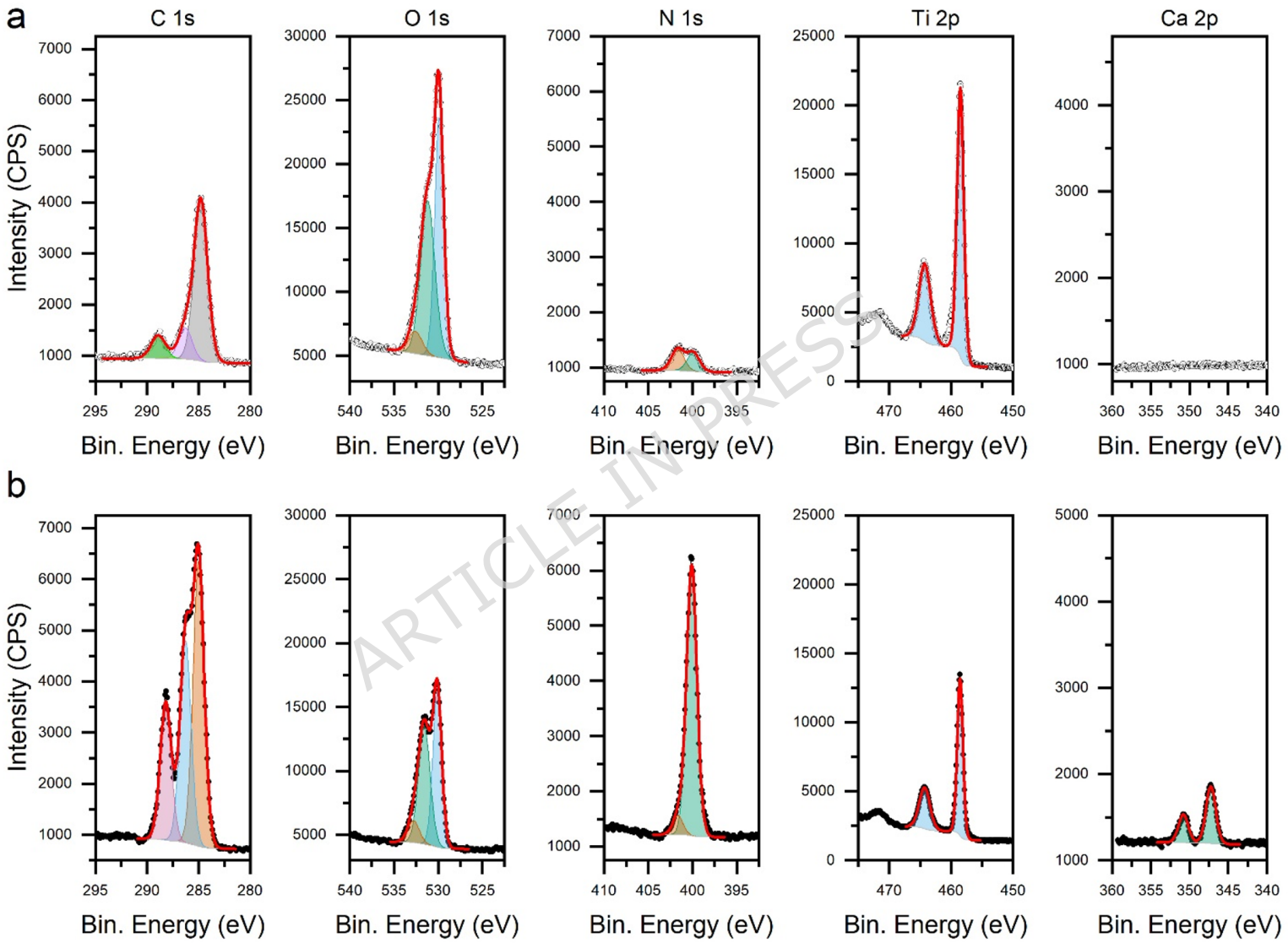

a

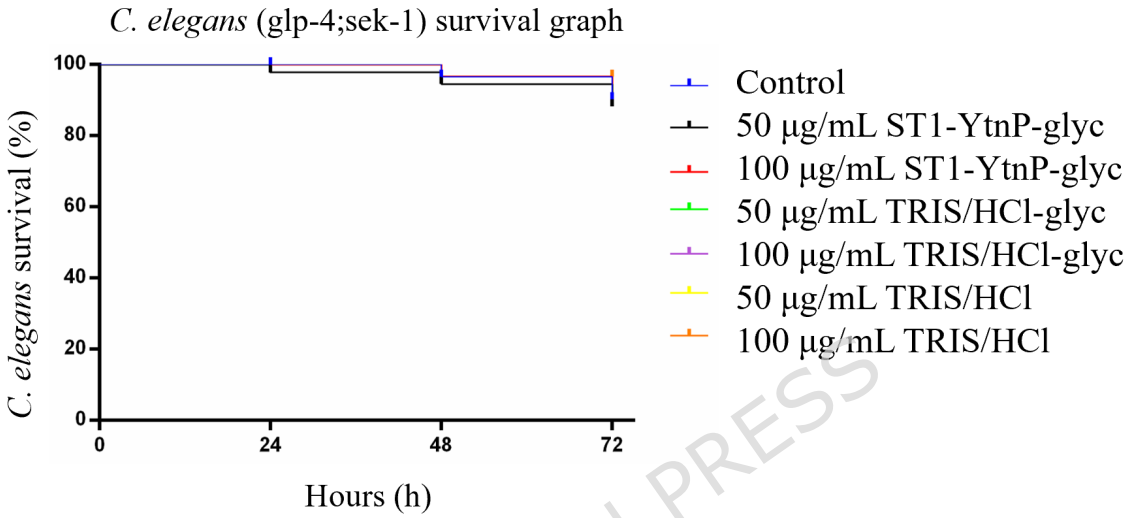

b

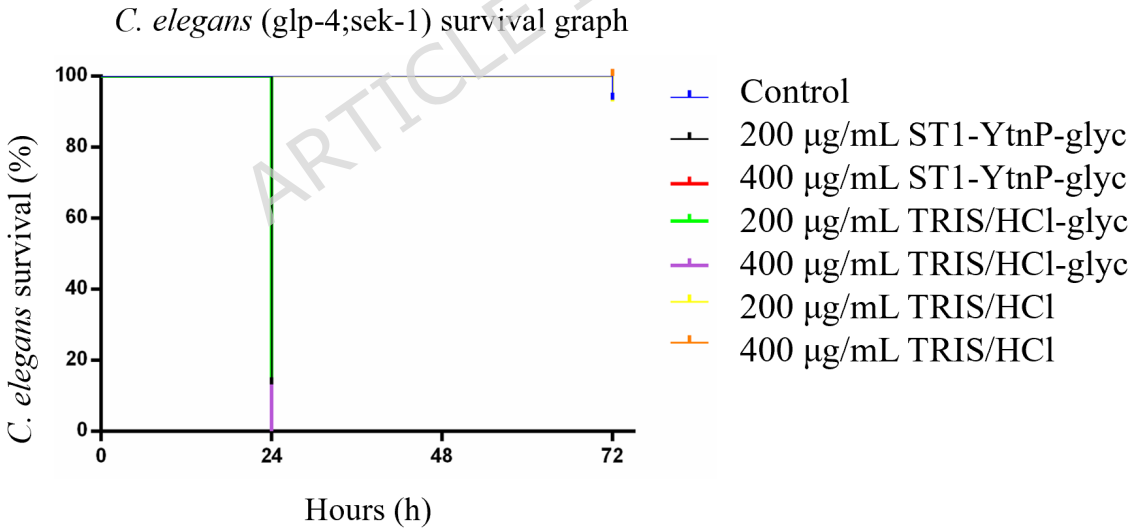

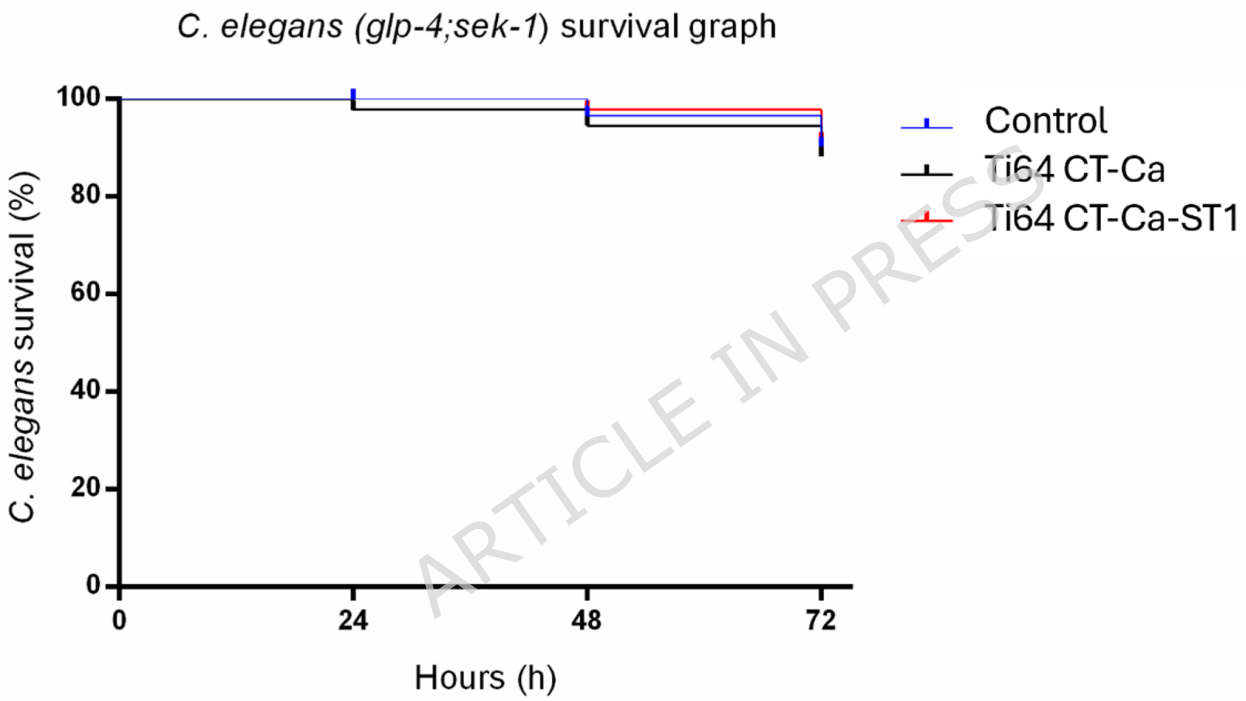

Sample	Contact Angle (°)	
Ti64 CT	63.9 ± 0	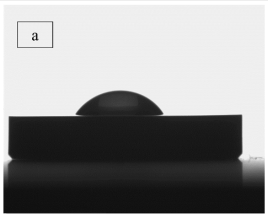
Ti64 CT-Ca	46.8 ± 17.1	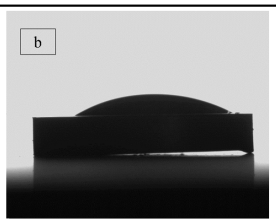
Ti64 CT-Ca-ST1	43.6 ± 8.5	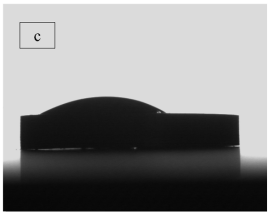

Sample	Elements (at%)				
	C	O	N	Ti	Ca
Ti64 CT	23.3	55.8	2.6	18.3	-
Ti64 CT-Ca ST1	47.1	31.4	13.1	7.7	0.7
ST1-YtnP (estimation)	32	10	9	-	-

	Ti64-CT		Ti64 CT-Ca-ST1	
	Binding Energy (eV)	%Area	Binding Energy (eV)	%Area
C-C, C-H	284.8 ± 0.2	75	285.0 ± 0.2	46
C-O	286.4 ± 0.2	14	286.2 ± 0.2	32
O-C=O	288.9 ± 0.2	11	288.0 ± 0.2	22

	Ti64-CT		Ti64 CT-Ca-ST1	
	Binding Energy (eV)	%Area	Binding Energy (eV)	%Area
O-Ti	529.9 ± 0.2	46	530.1 ± 0.2	46
-OH	531.2 ± 0.2	47	531.6 ± 0.2	45
C=O	532.6 ± 0.2	7	532.8 ± 0.2	9

	Ti64-CT		Ti64 CT-Ca-ST1	
	Binding Energy (eV)	%Area	Binding Energy (eV)	%Area
NH3+	401.7 ± 0.2	54	401.7 ± 0.2	7
NH2/(C=O)-NH-C	399.9 ± 0.2	46	400.1 ± 0.2	93

	Ti64-CT		Ti64 CT-Ca-ST1	
	Binding Energy (eV)	%Area	Binding Energy (eV)	%Area
Ti(IV)-O	458.5 ± 0.2	100	458.5 ± 0.2	100